applied optics

High-precision identification of a tip–tilt control system for the compensation of time delay

Yukun Wang,[1,2] Zhaoliang Cao,[1,*] Lifa Hu,[3] Xingyun Zhang,[1] Dayu Li,[1] Huanyu Xu,[1] Shaoxin Wang,[1] Quanquan Mu,[1] and Li Xuan[1]

[1]State Key Laboratory of Applied Optics, Changchun Institute of Optics, Fine Mechanics and Physics, Chinese Academy of Sciences, Changchun 130033, China
[2]Chinese Academy of Sciences University, Beijing 100039, China
[3]Jiangnan University, Wuxi 214122, China
*Corresponding author: caozlok@ciomp.ac.cn

Received 23 November 2016; revised 14 January 2017; accepted 15 January 2017; posted 17 January 2017 (Doc. ID 279990); published 8 February 2017

The resolution of ground-based large aperture telescopes is decreased severely due to the effect of atmospheric turbulence. Adaptive optics systems (AOSs) have been widely used to overcome this, and low-order aberrations [tip–tilt (TT)] are corrected by a TT mirror. In the tip/tilt TT correction loop, the time delay affects the correction performance significantly and a predicted signal compensation method (PSCM) has been used to reduce its effect. However, the performance of the PSCM is reduced obviously due to the low identification accuracy of the TT AOS model. In this paper, a nonlinear least squares subspace identification (NLSSI) method is presented to obtain a high-precision model of the TT AOS. The system is identified with the subspace method first, and then the identified parameters are modified in the frequency domain. By using this method, a TT correction system is identified. Compared with the subspace identification method, the identification accuracies of the time domain and frequency response are increased 2 and 5 times, respectively, with the NLSSI method. Furthermore, with the NLSSI method, the −3 dB error rejection bandwidth is increased from 69 to 76 Hz. Finally, an adaptive correction experiment is performed on a 1.23 m telescope, and the astronomical observation results show that the correction accuracy is increased to 1.5 times with the NLSSI method. Moreover, the peak intensity of the image is improved by 11% with the NLSSI method. This work is very helpful to improve the TT correction accuracy of AOS, particularly for extreme adaptive optics and faint target observation.

OCIS codes: (010.1080) Active or adaptive optics; (010.1285) Atmospheric correction; (220.1000) Aberration compensation.

https://doi.org/10.1364/AO.56.001431

1. INTRODUCTION

Adaptive optics systems (AOSs) have been widely used in large aperture telescopes to eliminate the effect of atmospheric turbulence [1–4]. Usually, a tip–tilt mirror (TTM) is used to correct the low-order aberrations (tip and tilt), and the high-order aberrations are corrected by a deformable mirror. For the aberrations caused by atmospheric turbulence, the low-order term accounts for 86.9% and it seriously affects the image resolution of the telescope [5]. In particular, extreme adaptive optics has been developed to observe subjects including exoplanets and super-massive black holes. This demands a Strehl ratio of the optical system of more than 90%, and then the correction error must be very small. All these applications require high-precision correction of the low-order aberrations.

The most common tip–tilt (TT) correction method is the simple and effective proportional integration differential (PID) control method [6,7]. To achieve a faster settling time of the TT correction system, the Type II control method is proposed [8]. To improve the correction accuracy, a linear quadratic Gaussian (LQG) control method is demonstrated [9], and the state of the atmospheric turbulence model is estimated with a Kalman filter. However, none of the above control methods solves the time delay problem. In all of the above control methods, the TT aberrations are detected by the wavefront sensor (WFS), and the detected signal is inaccurate due to the time delay in the TT correction loop. The TT aberrations have been changed while the TTM performs the TT correction, and, then, the correction accuracy will be decreased greatly. To solve this problem, many control methods have been investigated to decrease the effect of the time delay. First, an atmospheric-turbulence-prediction-based control method is presented to compensate time delay [10–15]. However, when the atmosphere turbulence gets stronger, the signal-to-noise ratio (SNR) of the WFS gets worse, which leads to low prediction validity

and instability of the AO control system. Recently, a predicted signal compensation method (PSCM) has been put forward to compensate time delay [16]. In this method, the prediction validity is sensitive to the accuracy of the TT control system model identified with the subspace method [16].

The subspace identification method is a powerful system identification method and it has been researched extensively. Based on the input–output data, the state space model may be directly identified by the subspace method [17]. Many researchers have proposed modified subspace methods [18–20]. To date, all of these methods are considered in the time domain. For an ideal system, the system model can be achieved accurately with the time-domain identification method or the frequency-domain identification method. However, because of the effect of random noise, an actual TT correction system model cannot be identified accurately with only the time-domain method or the frequency-domain method. Therefore, in this paper, we demonstrate a modified subspace method to improve identification accuracy: the TT correction system model is identified by the subspace method (a kind of time-domain method) first, and then is modified with the nonlinear least squares method in the frequency domain.

2. TT CORRECTION SYSTEM WITH PSCM

The scheme of the TT correction system with the PSCM is shown in Fig. 1. The TT correction system is composed of a WFS, a PSCM controller, a digital-to-analog converter (DAC), a high voltage amplifier (HVA), and a TTM. The residual aberration is detected by the WFS with detection noise n. The driving voltages of the TTM are computed with the PSCM controller and sent to the TTM through the DAC and HVA. Then, the TT aberrations of the atmospheric turbulence ϕ^{tur} will be compensated for by the correction response of the TTM ϕ^{cor}.

Because of the effect of the delay time τ, the TTM is fluctuating during the delay time, so the measured residual $e(k)$ is not accurate. To overcome this problem, the PSCM is presented and the movement of the TTM during the delay time is compensated for with the identified model $G(s)$ [16]. The mathematical expression of the PSCM controller can be described as

$$\begin{cases} v(k) = v(k-1) + k_1 e'(k) + k_2 e'(k-1) + k_3 e'(k-2) \\ e'(k) = e(k) + y(k) - y(k-nT) \end{cases}, \tag{1}$$

where $v(k)$ is the driving voltage, k_1, k_2, k_3 are the parameters of PID, $e(k)$ is the residual TT, $e'(k)$ is the residual TT with compensation, $y(k)$ is the output of the identified model $G_m(s)$, $y(k-nT)$ is the output of the identified model $G_m(s)$ with n steps delay, and n can be obtained by the analysis of working time sequence [16]. T is the sampling time. It can be seen that the accuracy of the identified model $G_m(s)$ has an important effect on the compensation of the time delay.

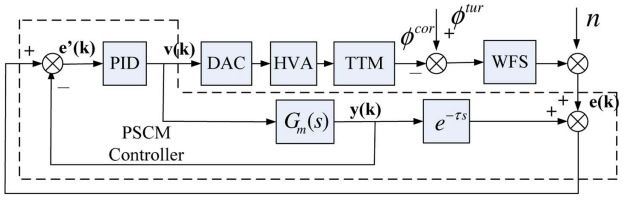

Fig. 1. Control scheme of the TT correction system.

For the above control system model, the system transfer function $G(s)$ is composed of $G_m(s)$ and delay time $e^{-\tau s}$. $G(s)$ can be described as [21]

$$\begin{aligned} G(s) &= \text{WFS}(s)\text{DAC}(s)\text{HVA}(s)G_{\text{ttm}}(s) \\ &= \left(\frac{1-e^{-Ts}}{Ts}\right)^2 k_{\text{HVA}} \frac{k_{\text{ttm}}}{s^2+\text{cs}+p} \\ &\approx \frac{Ke^{-Ts}}{s^2+\text{cs}+p} \\ &= G_m(s)e^{-Ts}, \end{aligned} \tag{2}$$

where k_{HVA} is the HVA gain, k_{ttm}, c, and p are the TTM parameters, $K = k_{\text{ttm}} \cdot k_{\text{HVA}}$, $(\frac{1-e^{-Ts}}{Ts})^2 \approx e^{-Ts}$, and the delay time τ is equal to sample time T.

Generally, the discrete system is described by a z transfer function ($z = e^{Ts}$), and then Eq. (2) can be transformed as Eq. (3) [22]:

$$G(z) = G_m(z)z^{-1} = \frac{b_1 + b_2 z^{-1} + b_3 z^{-2}}{a_1 + a_2 z^{-1} + a_3 z^{-2}} z^{-1}, \tag{3}$$

where $a_1, a_2, a_3, b_1, b_2, b_3$ are the parameters of the TT correction system model, and $\beta = (a_1, a_2, a_3, b_1, b_2, b_3)$ is defined to conveniently describe it. To obtain the identified model $G_m(s)$, the model parameter β should be achieved with the subspace identification method.

To overcome the effect of delay time with the PSCM, a high-precision model of TT correction is needed.

3. MODIFIED SUBSPACE IDENTIFICATION METHOD

Considering that an actual system cannot be identified accurately with only the time-domain method or frequency-domain method, we expect to improve the system model accuracy by combining the two methods. Concretely, the actual system is identified with the subspace identification method in the time domain first, and then the identification parameters are modified with the nonlinear least squares method in the frequency domain.

A. Subspace Identification

The subspace method [18–20] identifies the parameters with the state-space model. The state-space model can be described

$$\begin{cases} x(k+1) = Ax(k) + Bu(k) + Ke(k) \\ y(k) = Cx(k) \end{cases}, \tag{4}$$

where x is the vector of system state, and the dimension is 2×1. u is the input variable. y is the output variable. e is the identification error, and $[A, B, C, K]$ are the parameters for identification; A is a 2×2 matrix, B and K are vectors of 2×1, and C is a vector of 1×2.

The relation between current status variables and future input–output variables can be described as

$$\begin{cases} Y = O_f \cdot x(k) + T_f \cdot Z_f + E_f \\ Y = [y(k), y(k+1), \ldots, y(k+f-1)]' \\ Z_f = [u(k), y(k), \ldots, u(k+f-1), y(k+f-1)]' \\ E_f = [e(k), e(k+1), \ldots, e(k+f-1)]' \end{cases}, \quad (5)$$

where Y represents the future output variables, Z_f represents the combination of future input–output variables, and E_f is the identification error. O_f, T_f are the parameters of Eq. (5).

The relation between current status variables and past input–output variables can be described as

$$\begin{cases} O_f \cdot x(k) \approx H_p \cdot Z_p + E_p \\ Z_p = [u(k-p), y(k-p), \ldots, u(k-1), y(k-1)]' \\ E_p = [e(k-p), \ldots, e(k-1)]' \end{cases}, \quad (6)$$

where Z_p represents the combination of past input–output variables, E_p is the identification error, and H_p is the parameter of Eq. (6).

By combining Eqs. (5) and (6), a new relationship can be acquired:

$$\begin{cases} Y = [H_p, T_f] \cdot Z + E \\ Z = [Z_p; Z_f] \\ E = E_p + E_f \end{cases}, \quad (7)$$

With Eq. (7), H_p and T_f are estimated by using the linear least squares method. According to Eqs. (4) and (5), the system status x can be estimated by singular value decomposition of $H_p \cdot Z_p$. With the estimated x and Eq. (4), A, B, C can also be estimated by using the linear least squares method. The transform between Eqs. (3) and (4) can be described as

$$G(z) = C(zI - A)^{-1}B. \quad (8)$$

After transformation with Eq. (8), the state-space model can be transferred to a z transfer function, and then the model parameter β of Eq. (3) may be acquired. To improve the precision of identification, the achieved parameter β will be modified in the frequency-domain in the next section.

B. Frequency-domain Nonlinear Least Squares Modification

To describe the TT correction system in the frequency domain, Eq. (3) is changed into the frequency domain with $z = e^{j2\pi fT}$ as

$$G(f, \beta) = e^{-j2\pi fT} \frac{b_1 + b_2 e^{-j2\pi fT} + b_3 e^{-j4\pi fT}}{a_1 + a_2 e^{-j2\pi fT} + a_3 e^{-j4\pi fT}}. \quad (9)$$

Assuming the identified parameters obtained in time domain are β_0, $G(f, \beta)$ may be unfolded at β_0 by Taylor expansion as

$$G(f, \beta) = G(f, \beta_0) + G' \cdot (\beta - \beta_0) + R, \quad (10)$$

where G' is its first-order partial derivative at β_0, and R is the higher-order section.

Considering the effect of the random disturbance, the measured frequency response of the actual system can be defined as

$$G_m(f) = G(f, \beta) + \epsilon, \quad (11)$$

where $G_m(f)$ represents the measured frequency response, and ϵ represents the frequency response of the random disturbance. By combining Eqs. (10) and (11), $G_m(f)$ may be rewritten as

$$G_m(f) = G(f, \beta_0) + G' \cdot (\beta - \beta_0) + R + \epsilon. \quad (12)$$

Equation (12) may be transferred to a regression model as

$$G_m(f) - G(f, \beta_0) + G' \cdot \beta_0 = G' \cdot \beta + R + \epsilon. \quad (13)$$

Then, the model parameters may be solved according to Eq. (13) with the nonlinear least squares method and can be described as

$$\begin{aligned} \beta_1 &= (G'^T \cdot G')^{-1} \cdot G'^T \cdot (G_m(f) - G(f, \beta_0) + G' \cdot \beta_0) \\ &= \beta_0 + (G'^T \cdot G')^{-1} \cdot G'^T \cdot (G_m(f) - G(f, \beta_0)). \end{aligned} \quad (14)$$

Hence, the iterative formula of model parameters may be expressed as

$$\beta_{j+1} = \beta_j + (G'^T \cdot G')^{-1} \cdot G'^T \cdot (G_m(f) - G(f, \beta_j)). \quad (15)$$

The accurate model parameters can be acquired by using multiple iterations according to Eq. (15). Here, we define $Q = (R + \epsilon)^T (R + \epsilon)$ as the target function. Then, the available stopping rule is that the difference of $Q(\beta_{j+1}) - Q(\beta_j)$ is acceptable.

The initial model parameters β_0 can be achieved with the subspace method in the time domain. The frequency response $G_m(f)$ may be measured. With β_0 and $G_m(f)$, the accurate model parameters can be acquired by iteration with Eq. (15). As the nonlinear least squares method is utilized to do calculation, our method is called nonlinear least squares modified subspace identification (NLSSI).

4. SYSTEM IDENTIFICATION

A. Experimental Setup

To identify the TT correction system, a closed-loop control system is established in the laboratory, and its optical layout is shown in Fig. 2. The light output with a fiber bundle (the diameter is 200 μm, and the waveband is 400–700 nm) was collimated by lens L1 ($f = 80$ mm), the light diameter is limited at 7.8 mm with an iris aperture, and then reflected by the TTM. The reflected light is zoomed out by the combination of L2 ($f = 100$ mm) and L3 ($f = 73$ mm) and then detected by the WFS. The WFS is made by our group. The lens array of the WFS is 20 × 20, the focus of the lens array is 19.35 mm, the CCD dimension of the WFS is 120 × 120 pixels, and the pixel size of the CCD is 48 μm. In this optical design, the surface of the TTM conjugates with the microlens array of the WFS. A TTM (PI S334, with diameter of 10 mm) is used with the resonance frequency of 2.3 kHz. The sample rate of the WFS is set to 1.67 kHz.

B. Identification

To obtain the parameter β in the time domain, we must acquire the input–output data first. Ten-thousand random voltages

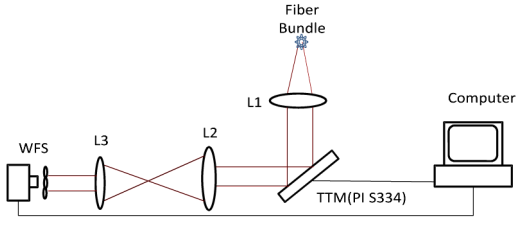

Fig. 2. Optical layout of the TT correction system.

were selected as the input data, and they are applied on one axis of the TTM with the range of −0.3 to 0.3 V. The corresponding responses were measured by the WFS as the output data. With Eqs. (5)–(8), the TT correction system model can be identified with the subspace method in the time domain. The result is shown in Fig. 3. The identification RMS error is 0.024 pixels. The model parameters are

$$G(z) = z^{-1}\frac{1.1477 - 0.5195z^{-1} - 0.5622z^{-2}}{1 - 0.9696z^{-1} + 0.0090z^{-2}}. \quad (16)$$

Based on the identified model parameter β in the time domain, the accuracy of the system model will be improved with the modification in the frequency domain. To measure the frequency response, a group of sinusoidal voltages were sent to the TTM with amplitude of 0.2 V. As TT aberrations with frequency of more than 300 Hz occupy the whole atmospheric turbulence with only the proportion of 0.0004% [5], it is sufficient to measure the frequency response with the frequency from 1 to 300 Hz. The sinusoidal response of the TTM is measured by the WFS as the output data. With these input–output data, the frequency response of the TT correction system $G_m(f)$ can be calculated by

$$G_m(f) = 20\log\left(\frac{\max(\text{output}(f)) - \min(\text{output}(f))}{\max(\text{in}put(f)) - \min(\text{in}put(f))}\right). \quad (17)$$

Then, with the calculated $G_m(f)$ and initial parameter β_0, which has been identified in the time domain, the modified parameter β may be acquired by iterating with Eq. (15), and the results are

$$G(z) = z^{-1}\frac{1.1312 - 0.5171z^{-1} - 0.5466z^{-2}}{1 - 0.9747z^{-1} + 0.0148z^{-2}}. \quad (18)$$

The output with Eq. (18) and the measured output are shown in Fig. 4. This indicates that, with the NLSSI method, the identification RMS error is 0.0085 pixels. Compared with the subspace method with identification error of 0.024 pixels, the identification accuracy is increased 2 times.

To compare with the subspace method in the time domain further, the identification results of the two methods in the frequency domain are shown in Fig. 5. It can be seen that the frequency response RMS errors are 0.025 and 0.15 dB, respectively, for the NLSSI and subspace methods. The identification accuracy of the frequency response is increased 5 times with the NLSSI method. Hence, the identification precision of the TT correction system can be obviously improved with the NLSSI method.

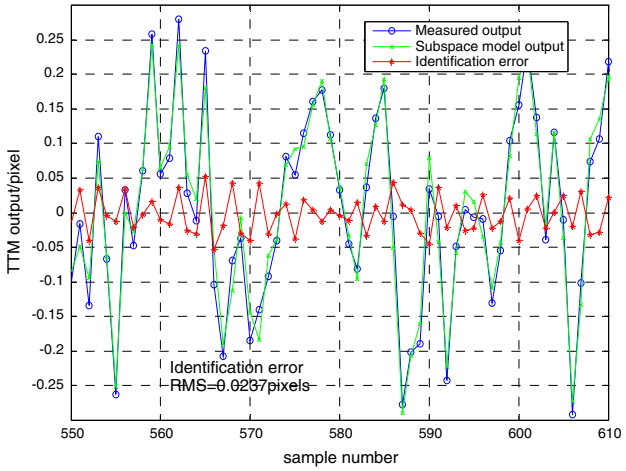

Fig. 3. Identification result of the subspace method in the time domain.

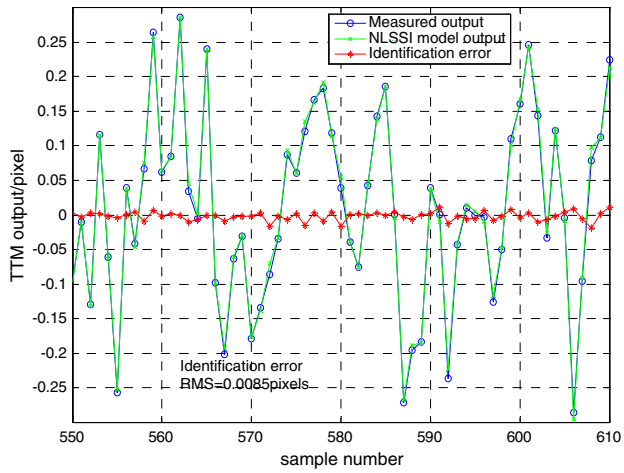

Fig. 4. Identification result of the NLSSI method in the time domain.

C. TT Correction System Bandwidth

Generally, the error rejection bandwidth is a criterion to evaluate the performance of a TT correction system. To measure the bandwidth of the TT correction, we add another TTM (PI S330) with lenses L4 ($f = 100$ mm) and L5 ($f = 100$ mm) to produce different sinusoidal frequency TT aberrations, and the new optical layout is shown in Fig. 6. The surfaces of TTM1 (PI 330) and TTM2 (PI S334), and the microlens array of the WFS are conjugated with each other.

First, a series of sinusoidal voltages from 1 to 300 Hz was sent to TTM1, and a WFS is utilized to measure the TT aberration as the disturbance data. Then, the TTM2 was used to

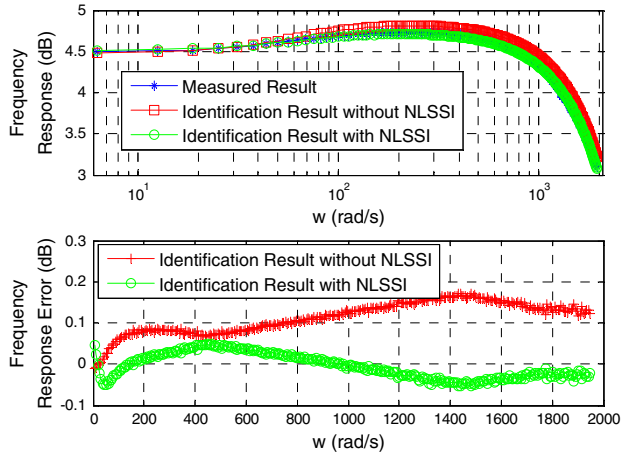

Fig. 5. Identification result in the frequency domain.

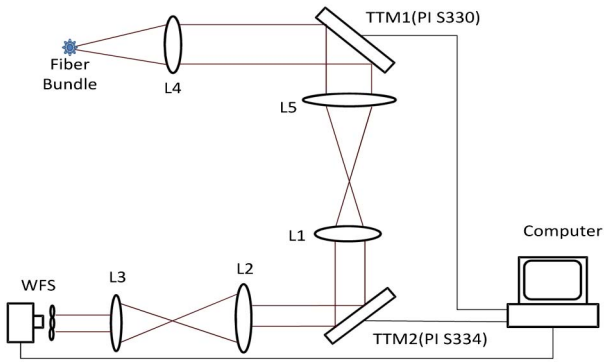

Fig. 6. Optical layout for system bandwidth measurement.

correct the TT disturbance, and the residual data is simultaneously measured by the WFS. With the measured data, the frequency response of the TT correction system can be calculated by

$$E(f) = 20\lg\left(\frac{\mathrm{std}(\mathrm{TT}_{\mathrm{residue}})}{\mathrm{std}(\mathrm{TT}_{\mathrm{disturbance}})}\right), \quad (19)$$

where std() means the standard deviation.

To do the comparison, the error rejection bandwidths are measured for the NLSSI and subspace methods, respectively, and the results are shown in Fig. 7. The results indicate that the −3 dB error rejection bandwidths are 76 and 69 Hz, respectively, for the NLSSI and subspace method. The −3 dB error rejection bandwidth is increased 10% with the NLSSI method. Therefore, the performance of the TT correction system is improved by using the modified identification method.

5. ADAPTIVE CORRECTION EXPERIMENT

To test the control performance of TT correction, an adaptive correction experiment of atmospheric turbulence was performed on a 1.23 m telescope with a liquid-crystal adaptive optics system (LCAOS) located in Changchun, China. Figure 8 shows the optical layout of the LCAOS. Polaris with a visual magnitude of 2.44 was observed on October 26, 2016, and the Greenwood frequency and atmospheric coherence length were measured as 58 Hz and 6 cm, respectively.

In the correction process, the low-order and high-order aberrations are corrected with the TTM and liquid-crystal wavefront corrector (LCWFC), respectively. The data of the TT aberrations obtained with the CCD camera were collected within 3 s during on-sky observation, as shown in Fig. 9. The exposure time of the CCD camera is 10 ms. During the first 1 s, the TT aberrations were not corrected; then the aberrations were corrected with the subspace and NLSSI methods, respectively, corresponding to the second and third seconds. It is shown that, after correction, the residual RMS errors of the TT aberrations had been reduced from 0.55 pixels to 0.38 pixels by using the NLSSI method, and the correction accuracy is increased to 1.5 times. As the TT aberrations of the atmospheric turbulence are dynamic, the image acquired with the CCD camera will be obscured due to exposure time integration. Figure 10 is the observed results on the CCD camera. Compared with the subspace method, the peak intensity is increased 11% with the NLSSI method. This is due to the improvement of low-order correction; therefore, the resolution of the image will be improved with the correction of the TT aberrations.

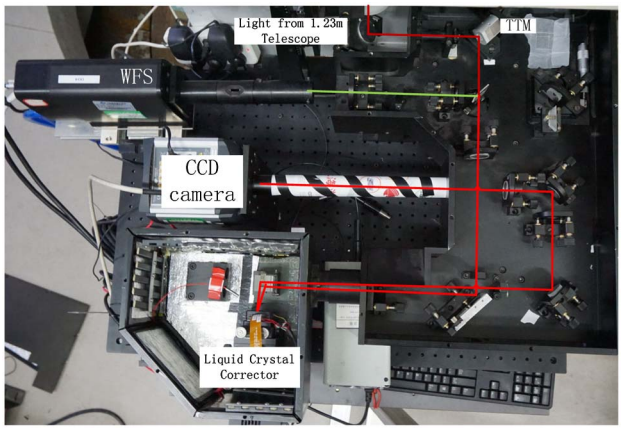

Fig. 8. Optical layout of LCAOS for the 1.23 m telescope.

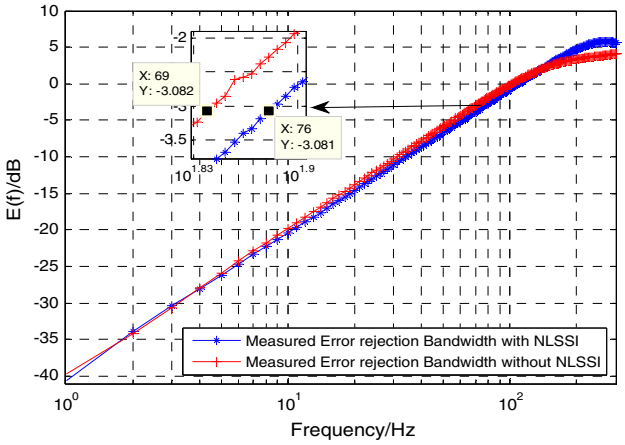

Fig. 7. Error rejection bandwidth of the PSCM with a different model.

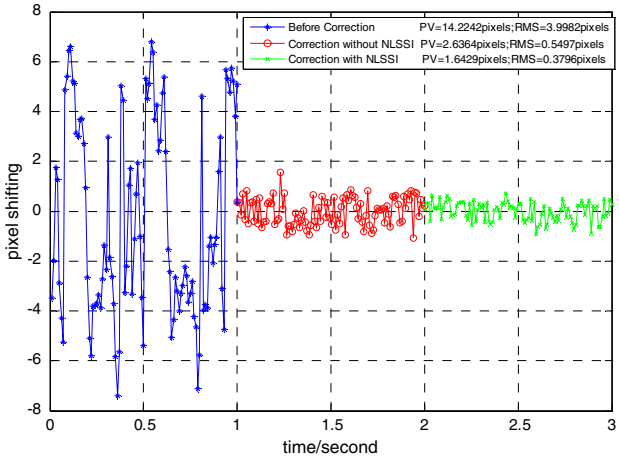

Fig. 9. On-sky TT aberration data obtained with the CCD camera.

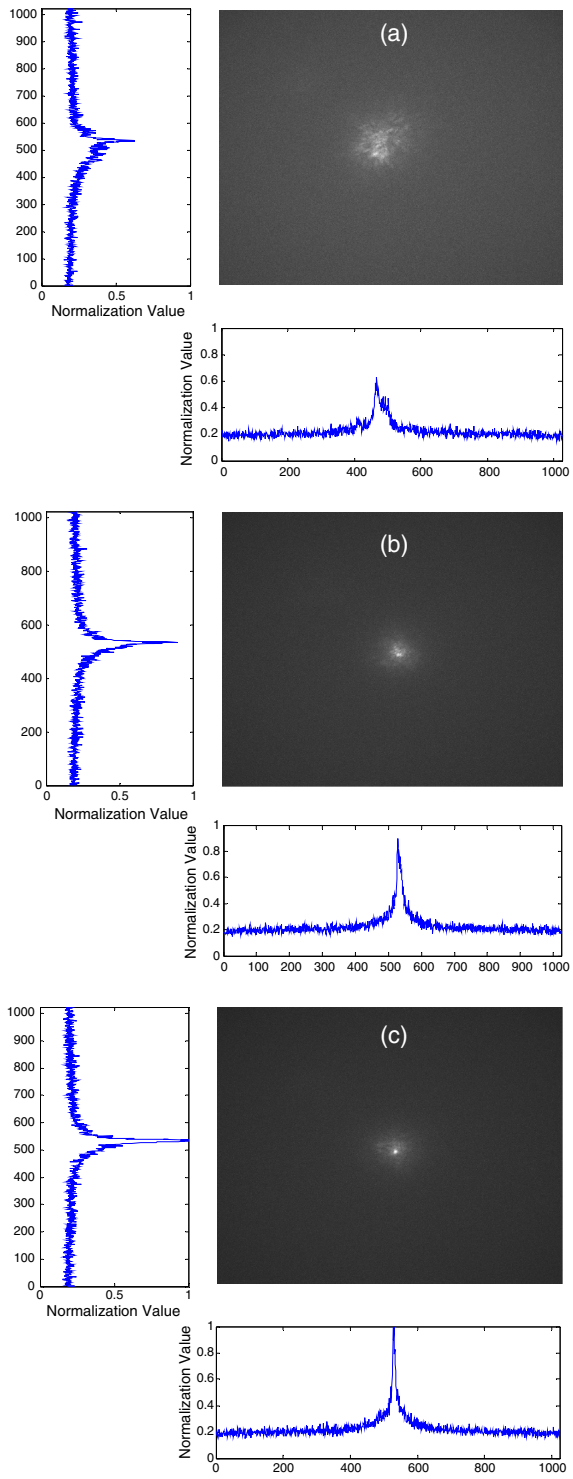

Fig. 10. Images of Polaris: (a) before correction, (b) after correction with the subspace method, and (c) after correction with the NLSSI method.

6. CONCLUSION

In this paper, we propose a NLSSI method to improve the identification accuracy of a TT correction system by which the performance of TT correction may be greatly improved. First, the theory of the NLSSI method is detailed. Then the model parameter is first identified with the subspace method, and then it is modified in the frequency domain with a nonlinear least squares method. Then, a TT correction system is established to perform the system identification. The identification results show that, with the NLSSI method, the identification RMS error of the time domain is decreased from 0.024 pixels to 0.0085 pixels, and the identification accuracy is increased 2 times. Meanwhile, the identification accuracy of the frequency response is increased 5 times with the NLSSI method. With the improved identification accuracy, the −3 dB error rejection bandwidth of the TT correction system is increased from 69 to 76 Hz. Hence, the NLSSI method can enhance the performance of the TT correction system.

Finally, to validate the NLSSI method, an adaptive correction experiment is done on a 1.23 m telescope. A star is observed and the atmospheric turbulence is corrected with the TTM and LCWFC. The residual RMS errors of the TT aberrations are reduced from 0.55 pixels to 0.38 pixels by using the NLSSI method and the correction accuracy is increased by a factor of 1.5 times. After correction, the peak intensity of the star image is increased by 11% by using the NLSSI method. Therefore, by using the NLSSI method, the performance of TT correction can be greatly improved.

Although a TTM is selected to do the identification, almost all the TT correction systems have similar performance, and the NLSSI method may be used to increase the performance of TT correction systems. This work will be useful to applications of AOSs, such as high-precision tracking of space objects, fainter target observation, and extreme adaptive optics.

Funding. National Natural Science Foundation of China (NSFC) (61377032, 61475152).

REFERENCES

1. J. W. Hardy, *Adaptive Optics for Astronomical Telescopes* (Oxford University, 1998).
2. M. Le Louarn, C. Vérinaud, V. Korkiakoski, N. Hubin, and E. Marchetti, "Adaptive optics simulations for the European extremely large telescope," Proc. SPIE **6272**, 627234 (2006).
3. E. Diolaiti, J.-M. Conan, I. Foppiani, E. Marchetti, A. Baruffolo, M. Bellazzini, G. Bregoli, C. R. Butler, P. Ciliegi, G. Cosentino, B. Delabre, M. Lombini, C. Petit, C. Robert, P. Rossettini, L. Schreiber, R. Tomelleri, V. Biliotti, S. D'Odorico, T. Fusco, N. Hubin, and S. Meimon, "Conceptual design and performance of the multi conjugate adaptive optics module for the European extremely large telescope," Proc. SPIE **7736**, 77360R (2010).
4. D. Harrington, S. Berdyugina, M. Chun, C. Ftaclas, D. Gisler, and J. Kuhn, "InnoPOL: an EMCCD imaging polar meter and 85-element curvature AO system on the 3.6-m AEOS telescope for cost effective polar metric speckle suppression," Proc. SPIE **9147**, 91477C (2014).
5. R. Noll, "Zernike polynomials and atmospheric turbulence," J. Opt. Soc. Am. A **66**, 207–211 (1976).
6. E. Fedrigo, R. Muradore, and D. Zilio, "High performance adaptive optics system with fine tip/tilt control," Control Eng. Pract. **17**, 122–135 (2009).
7. B. Sedghi, M. Müller, H. Bonneta, and B. B. Dimmlera, "Field stabilization (tip/tilt control) of E-ELT," Proc. SPIE **7733**, 773340 (2010).
8. K. Jackson, R. Conan, and J.-P. Véran, "Experimental validation of type II tip-tilt control in a woofer-tweeter adaptive optics system," Proc. SPIE **7736**, 77364K (2010).
9. C. Petit, J.-M. Conan, C. Kulcsár, H.-F. Raynaud, and T. Fusco, "First laboratory validation of vibration filtering with LQG control law for adaptive optics," Opt. Express **16**, 87-97 (2008).

10. B. Neichel, F. Rigaut, A. Guesalaga, I. Rodriguez, and D. Guzman, "Kalman and H-infinity controllers for GeMS," in *Imaging Systems Applications*, OSA Technical Digest (2011), paper JWA32.
11. Q. Fu, J.-U. Pott, D. Peter, F. Shen, C. Rao, and X. Li, "Experimental study on modified linear quadratic Gaussian control for adaptive optics," Appl. Opt. **53**, 1610-1619 (2014).
12. Y.-K. Wang, L.-F. Hu, C.-C. Wang, S.-X. Wang, and L. Xuan, "Adaptive inverse control for tip/tilt mirror in adaptive optics system," Opt. Precis. Eng. **23**, 2203–2210 (2015).
13. P. C. McGuire, T. A. Rhoadarmer, H. A. Coy, J. R. P. Angel, and M. Lloyd-Hart, "Linear zonal atmospheric prediction for adaptive optics," Proc. SPIE **4007**, 682–691 (2000).
14. M. B. Jorgenson and G. J. Aitken, "Prediction of atmospherically induced wave-front degradations," Opt. Lett. **17**, 466–468 (1992).
15. D. A. Montera, B. M. Welsh, M. C. Roggemann, and D. W. Ruck, "Prediction of wave-front sensor slope measurements with artificial neural networks," Appl. Opt. **36**, 675–681 (1997).
16. C. Wang, L. Hu, Y. Wang, S. Wang, Q. Mu, D. Li, Z. Cao, C. Yang, H. Xu, and X. Li, "Time delay compensation method for tip-tilt control in adaptive optics system," Appl. Opt. **54**, 3383–3388 (2015).
17. F. Chongzhi and X. Deyun, *Process Identification* (Tsinghua, 1988), Chap. 4.
18. M. Deistler, K. Peternel, and W. Scherrer, "Consistency and relative efficiency of subspace method," Automatica **31**, 1865–1875 (1995).
19. T. V. Gestel, J. A. K. Suykens, P. Van Dooren, and B. De Moor, "Identification of stable models in subspace identification by using regulation," IEEE Transition Autom. Control **46**, 1416–1420 (2001).
20. J. Wang and S. J. Qin, "A new subspace identification approach based on principle component analysis," J. Process Control **12**, 841–855 (2002).
21. C. Wang, L. Hu, H. Xu, Y. Wang, D. Li, S. Wang, Q. Mu, C. Yang, Z. Cao, X. Lu, and X. Li, "Wavefront detection method of a single-sensor based adaptive optics system," Opt. Express **23**, 21403–21413 (2015).
22. D. P. Looze, "Discrete-time model of an adaptive optics system," J. Opt. Soc. Am. A **24**, 2850–2863 (2007).